Supporting Information

Theoretical Investigation of Thermoelectric Properties of Methyl Blue-Based Molecular Junctions

Sarah M. S. Al-Mohana[ab], Hussein N. Najeeb[c], Rasool M. Al-Utayjawee[d] , Ferydon Babaei[a], Oday A. Al-Owaedi*[cf]

[a]Department of Physics, Faculty of Science, University of Qom, Qom, 3716146611, Iran.
[b]Iraqi Ministry of Education, Baghdad, 10074, Iraq.
[c]Department of Laser Physics, College of Science for Women, University of Babylon, Hilla 51001, Iraq.
[d]Iraqi Ministry of Education, Najaf Education Directorate, Najaf, 54001, Iraq.
[f]Al-Zahrawi University College, Karbala, Najaf-Karbala Street, 56001, Iraq.

*E-mail: oday.alowaedi@uobabylon.edu.iq

SIESTA and GOLLUM Codes

All calculations in this work were carried out by the implementation of DFT in the SIESTA code. [1] DFT have been used to obtain the optimized geometries of molecules and to carry out the iso-surfaces calculations to investigate their electronic properties using Gaussian [2] software at the B3LYP level of theory [3] with 6-31G** basis set. [4,5] SIESTA is an acronym derived from the Spanish Initiative for Electronic Simulations with Thousands of Atoms. GOLLUM is a program that computes the charge, spin and electronic contribution to the thermal transport properties of multi-terminal junctions. In contrast to a non-equilibrium Green's function (NEGF) codes, GOLLUM is based on equilibrium transport theory. All, theories and computational methods and procedures are shown in Figure S2.

The optimized geometry, ground state Hamiltonian and overlap matrix elements of each structure were self-consistently obtained using the SIESTA implementation, of the density functional theory (DFT). SIESTA employs norm-conserving pseudo-potentials to account for the core electrons and linear combinations of atomic orbitals to construct the valence states. The generalized gradient approximation (GGA) of the exchange and correlation functional is used with a double-ζ polarized (DZP) basis set, a real-space grid defined with an equivalent energy cut-off of 250 Ry. The geometry optimization for each structure is performed to the forces smaller than 20 meV/Å. The mean-field Hamiltonian obtained from the converged DFT calculation was combined with GOLLUM [6] implementation of the non-equilibrium Green's function method to calculate the phase-coherent, elastic scattering properties of the each system consist of left gold (source) and right gold (drain) electrodes and the scattering region. The transmission coefficient T(E) for electrons of energy E (passing from the source to the drain) is calculated via the relation:

$$T(E) = T_r\{\Gamma_R(E)G^R(E)\Gamma_L(E)G^{R\dagger}(E)\} \quad (1)$$

In this expression,

$$\Gamma_{L,R}(E) = i\left(\Sigma_{L,R}(E) - \Sigma_{L,R}^{\dagger}(E)\right) \quad (2)$$

$\Gamma_{L,R}$ describes the level broadening due to the coupling between left (L) and right (R) electrodes and the central scattering region, $\Sigma_{L,R}(E)$ are the retarded self-energies associated with this coupling.

$$G^R = \left(E\text{Ϫ} - H - \Sigma_L - \Sigma_R\right)^{-1} \quad (3)$$

G^R is the retarded Green's function, where H is the Hamiltonian and Ϫ is the overlap matrix (both of them are obtained from SIESTA). The transport properties is then calculated using the Landauer formula:

$$G(E_F T) = G_\circ \int_{-\infty}^{\infty} dE\, T(E)\left[-\partial f(E,T,E_F)/\partial E\right] \quad (4), \text{ where}$$

$$f = \left[e^{\left(E - E_F\right)/k_B T} + 1\right]^{-1} \quad (5)$$

is the Fermi-Dirac probability distribution function, T is the temperature, E_F is the Fermi energy, $G_\circ = (2e^2)/h$ is the conductance quantum, e is the electron charge and h is the Planck's constant. DFT can give inaccurate value for the Fermi energy that calculated conductance are obtained for a range of Fermi energies [7]. The thermopower or Seebeck coefficient S is defined as the difference of electrochemical potential per unit temperature difference developing across an electrically isolated sample exposed to a temperature gradient. The Seebeck coefficients and power factors is also informative. Providing of the transmission function, T(E), can be approximated by a straight line on the scale of K_{BT}, the Seebeck coefficient is given by:

$$S \approx -L|e|T\left(\frac{d\ln T(E)}{dE}\right)_{E = E_F} \quad (6)$$

Where L is the Lorenz number $L = \left(\frac{k_B}{e}\right)^2 \frac{\pi^2}{3} = 2.44 \times 10^{-8}\, W$. In other words, S is proportional to the negative of the slope of ln T(E), evaluated at the Fermi energy.

The power factor is the ratio of the real power absorbed by the load to the apparent power flowing in the circuit. Real power is the average of the instantaneous product of voltage and current and represents the capacity of the electricity for performing work. From the Seebeck coefficient, the power factor was calculated as given in equation (7).

$$P = GS^2 T \quad (7)$$

Where T is the temperature T = 300 K, G is the electrical conductance and S is the thermopower.

In conventional devices the maximum efficiency of either heat transfer or current generation is proportional to the dimensionless thermoelectric figure of merit. The common measure for thermoelectric efficiency is given by the figure of merit, which is given by: [8]

$$ZT = \frac{GS^2}{k_{el} + k_{ph}} T \quad (8)$$

Where G is the electrical conductance, S is the thermopower, k_{el} is the electron thermal conductance, $k_{ph}$is the phonon thermal conductance. The figure of merit is determined from the thermoelectric transport coefficients in equations 1, 9 – 10, and 12 in the linear response regime. [9–11]

$$G = \frac{2e^2}{h} k_0 \quad (9)$$

$$k_{el} = \frac{2}{hT}\left(K_2 - \frac{K_1^2}{K_0}\right) \quad (10)$$

In the expressions $e = |e|$ is the absolute value of the electron charge, h is the Planck constant, and $T = (T_L + T_R)/2$ is the average junction temperature. The coefficients in 9 and 10 are defined as:

$$k_n = \int dE\, T_{el}(E)\left(-\frac{\partial f(E)}{\partial E}\right)(E-\mu)^n \quad (11)$$

Where $T_{ph}(E)$ is the electron transmission, and the chemical potential $\mu \approx E_F$ is approximately given by the Fermi energy E_F of the Au electrodes. The corresponding thermal conductance due to the phonons is given in linear response by:

$$k_{ph} = \frac{1}{h}\int_0^\infty dE\, ET_{ph}(E)\frac{\partial n(E,T)}{\partial T} \quad (12)$$

Where $T_{ph}(E)$ is the phonon transmission and $n(E,T) = \{\exp(E/k_BT) - 1\}^{-1}$ is the Bose function, characterizing the phonon reservoirs in the left and right electrodes.

Hence, an upper bound for ZT in the limit of vanishing phonon thermal transport $\kappa_{ph} \rightarrow 0$ is given by the purely electronic contribution as

$$Z_{el}T = \frac{S^2 G}{k_{el}}T = \frac{S^2}{L} \quad (13)$$

Hence, the Lorenz number is $L = \kappa_{el}/GT$. With $Z_{el}T$, and depending on above the figure of merit is presented in a slightly different form as: [12]

$$ZT = \frac{Z_{el}T}{1 + {k_{ph}}/{k_{el}}} \quad (14)$$

Self-Consistent DFT Cycle

Density functional theory uses a self-consistent field (SCF) procedure. For example, let us suppose that E_{Hart} and E_{xc} can be accurately the effective single particle potential (V_{eff}) is determined. The problem is now that V_{eff} cannot be calculated until the correct ground state density is known and the correct density cannot be obtained from the Kohn-Sham wavefunctions until equation (15) is solved with the correct V_{eff}. This circular problem is solved by carrying out a self-consistent cycle [13–15], as shown in Figure S1.

$$[T_{non} + V_{eff}]\Psi_{K-S} = E\Psi_{K-S} \quad (15)$$

According to Figure S1, the first step is to generate the pseudo-potential which represents the electrostatic interaction between the valence electrons and the nuclei and core electrons. The next step is to build the required basis set with a selected kinetic energy cutoff to be inserted in the basis set; this step is to expand the density functional quantities. Clearly, if the density is known, the energy functional is fully determined. A trial electronic density $n^{initial}(\vec{r})$ is made as an initial guess. This initial guess is used to calculate the following quantity:

$$G = E_{Hart}\left[n^{initial}(\vec{r})\right] + E_{xc}\left[n^{initial}(\vec{r})\right] \quad (16)$$

Next step is to build the required basis set with a selected kinetic energy cutoff to be inserted in the basis set; this step is to expand the density functional quantities. Clearly, if the density is known, the energy functional is fully determined. A trial electronic density $n^{initial}(\vec{r})$ is made as an initial guess.

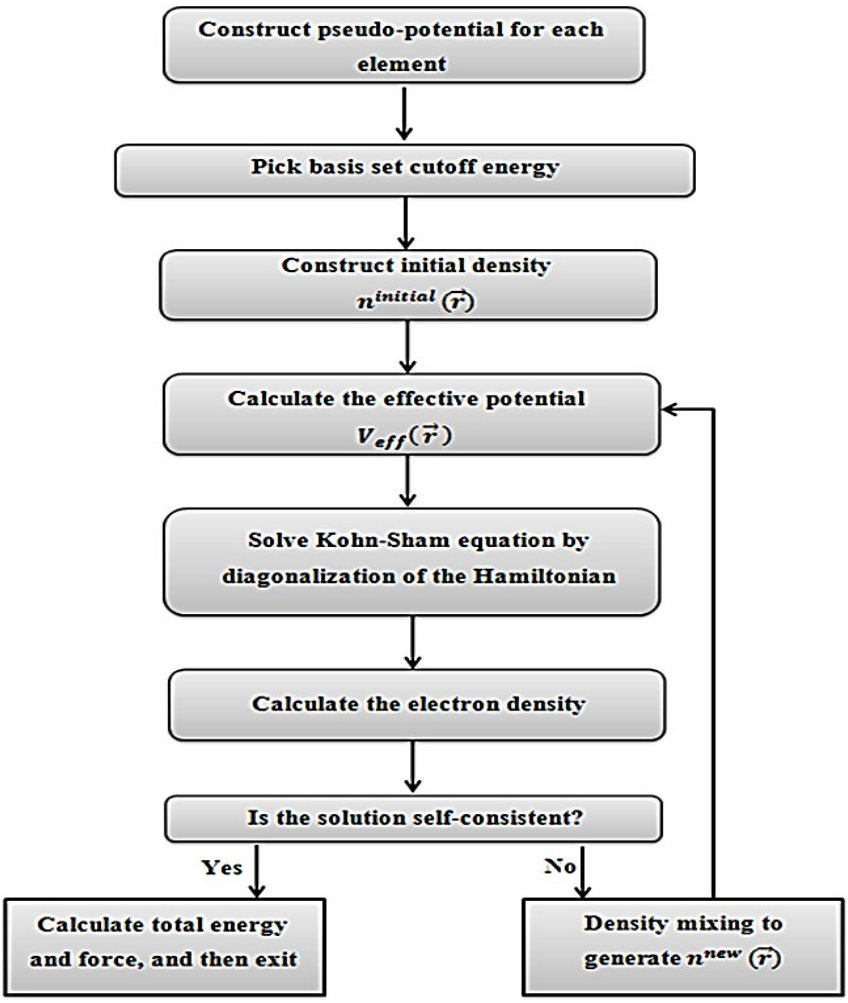

Figure S1. A Schematic illustration of the self-consistent DFT cycle. [14]

This initial guess is used to calculate the following quantity:

$$G = E_{Hart}\left[n^{initial}(\vec{r})\right] + E_{xc}\left[n^{initial}(\vec{r})\right] \quad (17)$$

Then $\frac{\partial G}{\partial n^{initial}(\vec{r})}$ and the effective potential V_{eff} are calculated. The effective potential is used to solve the Kohn-Sham equation (17) which leads to finding the electron Hamiltonian. After obtaining the Hamiltonian, it is diagonalized in order to find the eigenfunctions and the new electron density $n^{new}(\vec{r})$. Hopefully, this $n^{new}(\vec{r})$ will be closer to true ground state and is checked. For self-consistency, if this new updated electron density $n^{new}(\vec{r})$ agrees numerically with the density $n^{initial}(\vec{r})$ used to build the Hamiltonian at the beginning of the SCF cycle, we have reached the end of the loop. Final step is an exit, and calculate all the desired converged quantities, such as the total energy, the electronic band structure, density of states … *etc.* Otherwise, the new density $n^{new}(\vec{r})$ does not agree with the starting density $n^{initial}(\vec{r})$, one generates a new input density and starts another SCF cycle: build the new density-dependent Hamiltonian, solve and compute the density, and check for self-consistency. [13,14]

Calculations and Codes

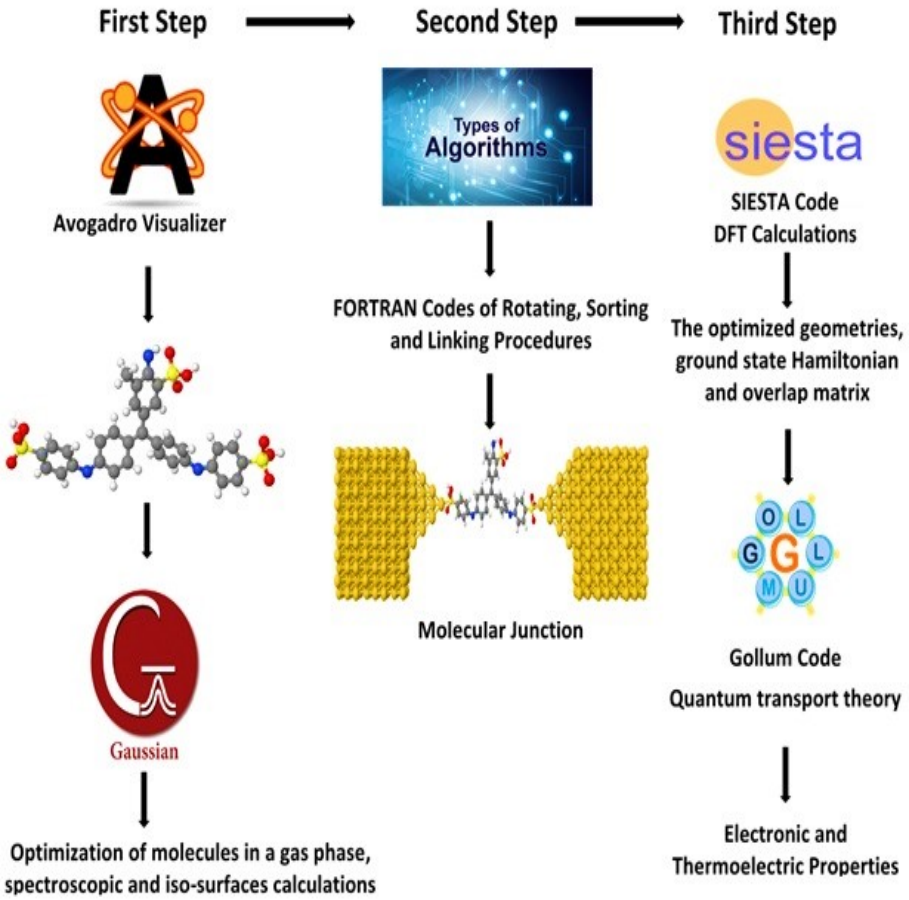

Figure S2. Theoretical calculations and codes.

All molecules in gas phase have been designed using Avogadro [16] visualizer, then the ground-state energy optimization of molecules and iso-surfaces calculations achieved using Gaussian [2] software at the B3LYP level of theory [3] with 6-31G** basis set. [4,5] The second step involves the rotation, sorting and linking the molecules to the gold electrodes to obtain the theoretical models of molecular junctions (see Figure S2), using a set of FORTRAN algorithms. After that the molecular junctions have been optimized using SIESTA. [13,17-19] The data (Hamiltonian and overlap matrix) was then fed to the Gollum [14] code, which

calculating the electronic and thermoelectric properties of all molecular junctions. All structural aspects [20] have been characterised using Jmol viewer as shown in Table S1.

References

1 J. P. Perdew, K. Burke, M. Ernzerhof, *Phys. Rev. Lett.* 1996, **77**, 3865.
2 H. B. Schlegel, J. S. Binkley, J. A. Pople. *J. Chem. Phys.* 1984, **80**, 1976-1981.
3 A. D. J. Becke, Chem. Phys. 1993, **98**, 5648-5652.
4 G. A. Petersson, A. Bennett, T. G. Tensfeldt, , M. A. Al-Laham, W. A.Shirley, J. Mantzaris, *J. Chem. Phys.* 1988, **89**, 2193-2198.
5 G. A. Petersson, M. A. J. Al-Laham, *Chem. Phys.* 1991, **94**, 6081-6090.
6 J. P. Perdew, Y. Wang, *Phys. Rev. B.* 1992, **45**, 13244.
7 C. J. Lambert, *Chem. Soc. Rev.* 2015, **44**, 875-888.
8 B. Marius, J. H. Thomas, P. Fabian, A. Yoshihiro, *Phys. Rev. B.* 2015, **91**, 165419.
9 U. Sivan, Y. Imry, *Phys. Rev. B.* 1986, **33**, 551.
10 K. Esfarjani, M. Zebarjadi, Y. Kawazoe, *Phys. Rev. B.* 2006, **73**, 085406.
11 K-H. Müller, *J. Chem. Phys.* 2008, **129**, 044708.
12 J. Ferrer, C. J. Lambert, V. M. García-Suárez, D. Zs Manrique, D. Visontai, L. Oroszlany, R. Rodríguez-Ferradás, I. Grace, S. W. D. Bailey, K. Gillemot, S. Hatef, L. A. Algharagholy, *New J. Phys.* 2014, **16**, 93029.
13 R. E. Sparks, V. M. Garcı´a-Sua´rez, C. J. Lambert, *Phys. Rev. B. Cond. Matt. Mat. Phys.* 2011, **83**, 075437.
14 M. D. Hanwell, D. E. Curtis, D. C Lonie, T. Vandermeersch, E. Zurek, G. R. Hutchison, *J. Chem. Inform.* 2012, **4**, 1-17.
15 S. Yoram, A. C. Marco, S. M. Theresa, L. A. David, *J. Am. Chem. Soc.* 2004, **126**, 13, 4052–4053.
16 M. L. Perrin, C. J. O. Verzijl, C. A. Martin, A. J. Shaikh, R. Eelkema, J. H. van Esch, J. M. van Ruitenbeek, J. M. Thijssen, H. S. van der Zant, D. Dulic, *Nat. Nanotechnol.* 2013, **8**, 282–287.
17 O. A. Al-Owaedi, *ACS Omega,* 2024, **9**, 10610–10620.
18 R. Davidson, O. A. Al-Owaedi, D. C. Milan, Q. Zeng, J. Tory, F. Hartl, S. J. Higgins, R. J. Nichols, C. J. Lambert, P. J. Low, *Inorg. Chem.* 2016, **55**, 2691–2700.
19 R. J. Davidson, D. C. Milan, O. A. Al-Owaedi, A. K. Ismael, R. J. Nichols, S. J. Higgins, C. J. Lambert, D. S. Yufita, A. Beeby, *RSC Adv.* 2018, **8**, 23585-23590.
20 B. A. A. Al-Mammory, O. A. Al-Owaedi, E. M. Al-Robayi, *J. Phys.: Conf. Ser.* 2021, **1818**, 01209.